ISSN 1990-7931, Russian Journal of Physical Chemistry B, 2020, Vol. 14, No. 4, pp. 697–704. © Pleiades Publishing, Ltd., 2020.
Russian Text © The Author(s), 2020, published in Khimicheskaya Fizika, 2020, Vol. 39, No. 7, pp. 63–71.

CHEMICAL PHYSICS OF NANOMATERIALS

Morphology and Adsorption Properties of Bimetallic Nanostructured Coatings on Pyrolytic Graphite

M. V. Grishin[a,*], A. K. Gatin[a], S. Yu. Sarvadii[a], V. G. Slutskii[a], B. R. Shub[a], A. I. Kulak[b], T. N. Rostovshchikova[c], S. A. Gurevich[d], V. M. Kozhevin[d], and D. A. Yavsin[d]

[a]*Semenov Institute of Chemical Physics, Russian Academy of Sciences, Moscow, 117977 Russia*
[b]*Institute of General and Inorganic Chemistry, National Academy of Sciences of Belarus, Minsk, Belarus*
[c]*Moscow State University, Moscow, 119991 Russia*
[d]*Ioffe Physical Technical Institute, Russian Academy of Sciences, St. Petersburg, 194021 Russia*
**e-mail: mvgrishin68@yandex.ru*

Received April 26, 2019; revised May 19, 2019; accepted May 20, 2019

Abstract—The paper presents the results of studies of coatings formed by gold, copper, nickel, and palladium nanoparticles in various combinations on the surface of highly oriented pyrolytic graphite. It was shown that the structure of the bimetallic coatings and the adsorption of hydrogen, oxygen, and carbon monoxide on them are affected by interactions between dissimilar nanoparticles.

Keywords: nanostructured coatings, gold, copper, nickel, palladium, hydrogen, oxygen, carbon monoxide, hydrogen, adsorption

DOI: 10.1134/S1990793120040065

INTRODUCTION

Bimetallic catalysts exhibit high catalytic activity in various chemical reactions [1]. The catalysts based on gold and copper nanoparticles are widely used, for example, in the oxidation of various hydrocarbons: benzyl alcohol, propylene, methanol, and others [2–9], and in the low-temperature oxidation of CO [10–12]. The composites consisting of mixtures of gold and nickel nanoparticles were shown to have higher activity than the single-component nanostructured gold and nickel catalysts in steam reforming and CO oxidation [13] and in cross-condensation of alcohols [14]. The use of Au–Ni catalysts increases the yield of allylbenzene isomerization products [15]. These catalysts are characterized by increased activity and stability in hydrodechlorination processes [16].

Nickel-palladium catalysts are characterized by high activity, selectivity, and stability in many redox processes [17, 18]. The $Ni_{0.4}Pd_{0.6}$ catalysts participate in direct synthesis of H_2O_2 and surpass the monometallic palladium catalyst in stability and selectivity [19]. The addition of palladium to nickel in a ratio of 3 : 7 allows synthesis of an effective catalyst for the decomposition of hydrazine into simple substances [20]. NiPd nanoparticles have increased catalytic activity compared to Pd particles, for example, in cross-coupling of vinyl and aryl halides with terminal alkynes [21], hydrogenation of a number of nitro-substituted aromatic hydrocarbons under mild conditions [22], hydrogen energy processes [23], and hydrodechlorination of chlorohydrocarbons [24]. Thus, bimetallic coatings can become the basis of new, more efficient systems. At the same time, the factors governing the unique properties of bimetallic catalysts remain unknown, although this problem has already been solved for some coatings [25].

To examine the reasons for differences in the physicochemical properties of bimetallic systems and monometallic analogs and to search for conditions for their effective use in catalysis requires knowledge of the structure of these materials. The methods used for this purpose generally include transmission electron microscopy (TEM), X-ray phase analysis (XRD), X-ray photoelectron spectroscopy (XPS), IR spectroscopy, and visible spectroscopy [13, 26–28]. However, the information obtained by these methods is averaged over various nanoparticles, which makes it difficult to determine the mechanisms of chemical reactions. The use of scanning tunnel microscopy combined with tunnel spectroscopy (STM/STS) makes it possible not only to determine the size and shape of individual nanoparticles, but also to obtain information on their electronic structure, identify the molecules adsorbed on them, and reveal interparticle interaction effects (synergism) [29–32]. The goal of this study was to determine the morphology and local electronic structure of gold-copper, gold-nickel, and nickel-palladium nanostructured coatings on graph-

Table 1. Effect of adsorption on the electronic structure of nanoparticles from the gold-copper coating

Treatment	Percent of nanoparticles with different types of CVCs, %		
	type 2	type 3	type 4
Initial state	27	42	31
Exposure in CO	20	57	23
Exposure in H	4	39	37
Exposure in O_2	24	22	53

ite, and also the laws governing the interaction of these coatings with H_2, O_2, and CO gases.

EXPERIMENTAL

The Au and Cu, as well as Au and Ni, nanoparticles were deposited by impregnation. The aqueous $HAuCl_4$, $Ni(NO_3)_2$, or $Cu(NO_3)_2$ solutions with a metal concentration of 2.4×10^{-8} g/L in different combinations were simultaneously deposited on the surface of highly oriented pyrolytic graphite (HOPG), dried, and heated for a few hours at $T = 500$–750 K under ultrahigh vacuum. The NiPd coatings on the HOPG surface were prepared by laser electrodispersion (LED) [34] of an alloy containing 65 wt % Ni and 35 wt % Pd similar to that studied in [24].

The local and electronic structure of nanostructured coatings were analyzed by ultrahigh vacuum scanning tunneling microscopy (STM). The measurement of the current-voltage (CV) characteristics (curves) of STM nanocontacts containing nanoparticles deposited on a substrate (hereinafter, CVCs of nanoparticles) allows us to analyze the results of the action of adsorbed molecules on the surface of nanoparticles. For example, the CVCs of pure gold nanoparticles have an S shape typical of a tunneling contact of two metals with a nonzero derivative in the vicinity of zero voltages. After exposure to hydrogen, a region with zero conductivity appears on the CVCs of these nanoparticles [35]. After exposure to gases, other significant changes in the shape of CVCs occasionally took place, namely, local maxima appeared, with voltage intervals between them dU being numerically equal to the energy of the characteristic vibrational quantum of the adsorbed particle, $h\nu$: $edU = h\nu$, where e is the elementary charge [31]. To determine the local characteristics of the coatings, topographic and spectroscopic measurements were performed on four or five nonadjacent sections of the sample surface of sizes 150–500 nm, which contained a few dozens of nanoparticles. For correct interpretation, the CVCs of nanoparticles were compared with Auger spectroscopy data.

The residual gas pressure in the STM chamber did not exceed $P = 2 \times 10^{-10}$ Torr, which made it possible to exclude an uncontrolled change in the chemical composition of the samples and ensured reliability of the obtained information. To determine the adsorption characteristics, the samples containing nanoparticles were exposed in H_2, O_2, and CO at $P = 1 \times 10^{-6}$ Torr and $T =$ 300 K for the time required to achieve the required exposure. The exposure was measured in Langmuirs (1 L = 1×10^{-6} Torr s). All further topographic and spectroscopic measurements were performed after the gas was removed from the unit. The elemental composition of the samples was also determined by Auger spectroscopy. The chemical composition of the gaseous medium of the ultrahigh vacuum chamber was controlled with a quadrupole mass spectrometer at all stages of operation.

RESULTS AND DISCUSSION

Gold-Copper Coating

The HOPG surface contains clusters of spherical nanoparticles (diameter 2–6 nm), located mainly on the edges of graphene sheets (Fig. 1a). The nanoparticles cover up to 15% of the sample surface. The CV measurements revealed three types of nanoparticles, which differed significantly in their electronic structure (curves *2*–*4*, Fig. 1b). A quantitative analysis of CVCs of various types showed that nanoparticles that correspond to the CVCs of curve *3* in Fig. 1b (type 3) are dominant in the gold-copper coating. These are ~40% of the total number of nanoparticles. The number of nanoparticles that correspond to CV curve *2* in Fig. 1b (type 2) and CV curve *4* in Fig. 1b (type 4) is approximately the same, ≈30% (Table 1). The data on the types and number of observed curves were compared with the experimental data for monometallic gold or copper coatings [36]; the results of this comparison and the fact that nanoparticles do not form multilayer clusters under the conditions of our experiment suggested that type *2* curves most likely correspond to gold nanoparticles; type *3* curves, to copper nanoparticles containing no oxygen atoms on their surface; and type *4* curves, to oxidized copper nanoparticles. Indeed, the results of XPS studies [37] showed that in gold-copper systems similar to those studied here, gold is in the Au^0 state, and copper is in the Cu^0 and Cu^{2+} states, which agrees with our data.

The marked asymmetry of CVCs with current locking in the region of positive displacements (curve *4*) may be explained by the fact that copper oxides are typical *p*-type semiconductors with a band gap of 2.1–2.2 eV for Cu_2O and 1.0–1.4 eV for CuO [38, 39]. The presence of copper oxides along with reduced copper Cu^0 is probably due to the peculiarities of its deposition by thermal decomposition of copper nitrate on the HOPG surface. In this process, CuO particles initially form [40], which are then reduced to Cu^0 as a result of oxygen loss under ultrahigh vacuum. In view of the relatively low heating temperature (500–750 K),

which is clearly insufficient for the formation of a stable crystal lattice inherent in metallurgical copper or high-temperature copper oxide, one would expect topotaxy effects, which cause high defectiveness and, accordingly, reactivity of the forming particles. It was found [41, 42] that under conditions when one of the components of the system is oxidized, mixed particles (alloys) do not form; i.e., the formation of AuCu nanoparticles in the presence of oxygen is unlikely. In addition, the possibility of pure gold and copper nanoparticles on the surface of reduced graphene oxide was reported in [11] and [43].

The exposure of the nanostructured gold-copper coating in CO led to a change in the ratio between nanoparticles with different electronic structures, i.e., between those that differ in the form of CVC. The number of nanoparticles with CVC of type 3 (pure copper) drastically increased, and the number of nanoparticles with CVC of type 4 (oxidized copper) decreased (Table 1); i.e., the oxide was reduced. As a result of the interaction of surface oxygen with adsorbed CO molecules with formation and subsequent desorption of CO_2 molecules, the electronic structure of the surface transforms from semiconductor to metal type. Similar results were obtained for catalytic systems including AuCu/CuO nanoparticles [43]. The authors noted that the presence of copper oxide (CuO) is favorable for CO oxidation, while the AuCu system is inactive in this reaction.

The effect of hydrogen on the electronic structure of nanoparticles shows itself in two ways. According to Table 1, the number of nanoparticles with CVCs of type 4 (i.e., nanoparticles with a semiconductor electronic structure of the surface) dramatically increased, while the number of pure gold (type 2 curves) and pure copper (type 3 curves) nanoparticles decreased. The results presented in [35] showed that hydrogen not only reduced the oxidized copper nanoparticles, but also caused the transformation of their electronic structure from metal to semiconductor type while being adsorbed on gold and oxide-free copper nanoparticles. This transformation may be associated with the semiconductor nature of copper hydrides and AuH, which form due to the high reactivity of copper and gold particles. As is known, copper hydride CuH with a wurtzite structure is characterized by *p*-type conductivity and has a band gap *E*g of 0.53–0.64 and 1.26 eV [45] (calculations using the PBE and PBE0 functionals, respectively); 0.65–0.68 [46], 0.74 eV [47]. Despite the instability of copper and especially gold hydrides, their formation seems quite possible in view of the high activity of the starting copper and gold nanoparticles. Thus, after exposure to hydrogen, the group of particles with type 4 CVCs included not only the remaining oxidized copper nanoparticles, but also copper and gold nanoparticles whose surface contains hydrogen adatoms. The sequential exposure of the sample to H_2 and CO (and vice versa) at room temperature did not lead to the interaction of these gases with each other on the surface of nanoparticles: no traces of adsorption of molecules with C–H and C–O bonds were detected by STM.

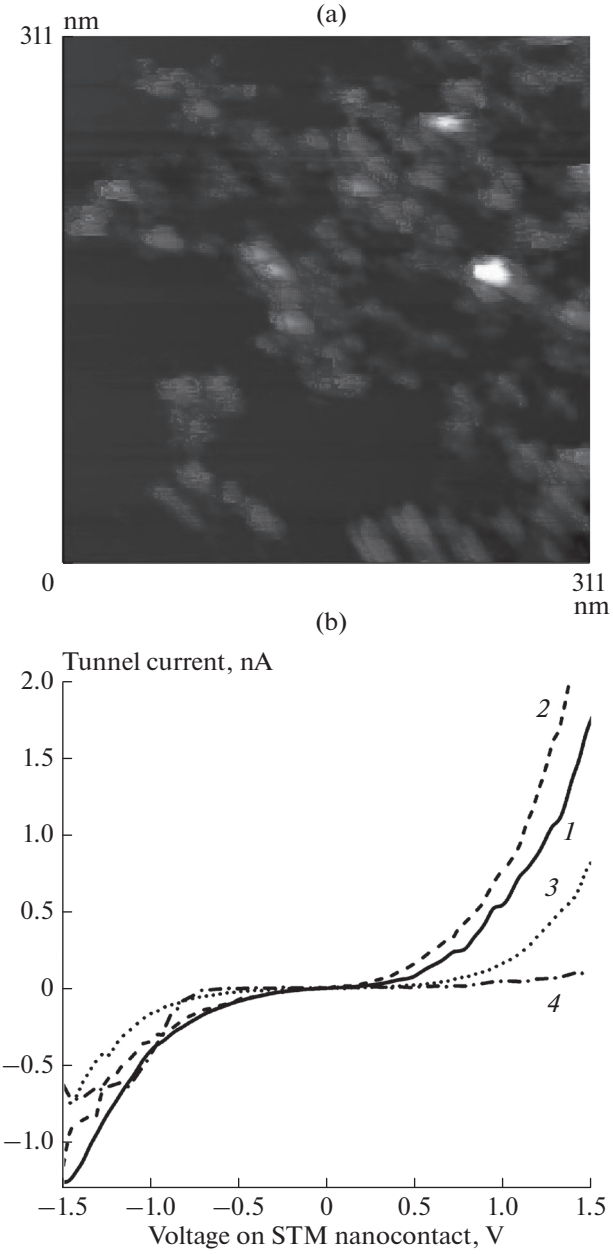

Fig. 1. Clusters of Au and Cu nanoparticles on HOPG: (a) topographic image of a region of the sample surface, and (b) examples of CVCs of (*1*) HOPG and (*2–4*) nanoparticles.

The results obtained after exposure to oxygen of the gold-copper coating, which was previously exposed to carbon oxide and then to hydrogen, are also presented in Table 1. On the one hand, the number of particles with CVC of type 4 increased; on the other hand, the number of particles with CVC of type 2 also increased

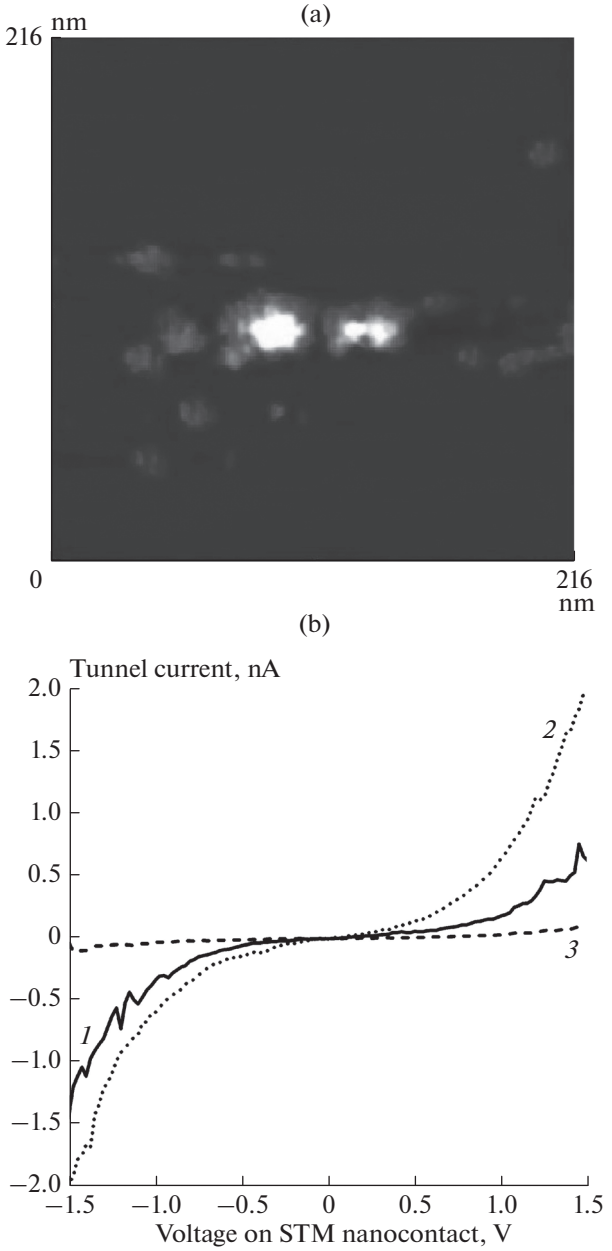

Fig. 2. (a) Image of nanoparticle clusters on HOPG and (b) spectral data for (*1*) HOPG and (*2*, *3*) nanoparticles that form the bimetallic AuNi coatings.

dramatically. This is evidently due to two processes occurring simultaneously on Au nanoparticles coated with hydrogen adatoms and pure Cu nanoparticles. Firstly, Au nanoparticles got rid of adsorbed hydrogen; secondly, copper nanoparticles with CVC of type 3 were oxidized. Also note that when the surface of Au nanoparticles is freed from hydrogen atoms, the latter is desorbed mainly as a part of H_2O molecules. This means that in the presence of copper (or copper oxide), as well as in the presence of oxidized nickel nanoparticles [48], two-stage synthesis of water occurs during the adsorption of hydrogen and oxygen. In contrast, the formation of water on gold nanoparticles on HOPG requires preliminary activation of the sample with hydrogen; i.e., water formation occurs in three stages only during the sequential adsorption of hydrogen, oxygen, and again hydrogen [35].

Gold-Nickel Coating

Figure 2a shows an image of a surface region of HOPG with nearly spherical nanoparticles with diameters of 2–3 and 4–6 nm, which covered 5–7% of its surface. The majority of nanoparticles are part of clusters consisting of nanoparticles that are close in diameter (homogeneous clusters) and nanoparticles that differ in diameter (heterogeneous clusters). CV measurements on nanoparticles of different sizes showed that the particles with diameters of 4–6 nm corresponded to S-shaped CVCs (curve *2*, Fig. 2b); the particles with diameters of 2–3 nm corresponded to Z-shaped CVCs with a zero current region with a width of 2 V (curve *3*, Fig. 2b). Earlier [49], we found that gold nanoparticles did not contain impurities, and their electronic structure was of metallic type. At the same time, nickel nanoparticles are oxidized and, accordingly, are of semiconductor type (the band gap of *p*-type nickel oxide, *p*-NiO, is E_g = 3.4–3.6 eV [50, 51]). This suggests that larger nanoparticles consisted of gold, and smaller nanoparticles, of nickel combined with nickel oxide. As in the process of formation of copper particles, initially, during the thermal decomposition of $Ni(NO_3)_2$, nickel nanoparticles are generated in the form of NiO oxide (at 573 K according to the data of [52]) and then the latter can transform into Ni^0. Even more pronounced topotactic effects should be expected in this process [53] than those in the course of copper oxide reduction due to the higher thermal stability of nickel oxide.

Thus, the use of spectroscopic measurements in STM made it possible to separate nanoparticles of similar sizes but different elemental compositions in the same coating.

The adsorption properties of the nanostructured gold-nickel coating were determined relative to H_2, CO, and O_2. The exposure of the bimetallic coating in hydrogen led to the same results as in the case of gold and nickel nanoparticles separately. The electronic structure of Au nanoparticles transformed from metal to semiconductor type, and nickel oxide was partially reduced (curves *1*, Figs. 3a and 3b). As a result of subsequent exposure of the gold-nickel coating previously stored in H_2, a fairly large number of series of local maxima with voltage intervals dU_1 = 0.2 V and dU_2 = 0.3 V appeared in CO on the CVCs of Au nanoparticles (curve *2*, Fig. 3a). The coincidence of the results of these measurements with the IR spectroscopy data [54] suggests that the observed features are caused by vibronic excitation of the C–O and C–H bonds, respec-

tively. By analogy with the data of [55], it can be assumed that formyl radicals (HCO•) formed on gold, as on the nanostructured Au coating [49]. At the same time, the exposure to CO led to complete reduction of the oxidized surface of the overwhelming majority of nickel nanoparticles (curve *2*, Fig. 3b). Indeed, the energy barrier of the reaction $CO + NiO \rightarrow Ni + CO_2$ is only 0.4 eV; therefore, it could occur under the conditions of our experiment. The exposure of the sample to O_2 led to almost complete disappearance of the series of local maxima with intervals of $dU_1 = 0.3$ V and simultaneous significant increase in the number of these curves with $dU_2 = 0.2$ V (curve *3*, Fig. 3a). According to the data of [56], this value of vibronic quantum could also relate to the excitation of C=O bonds in the CO_2 molecule. In addition to the CVCs of nanoparticles described above, which had features caused by vibronic excitation of CO_2, the curves with series of local maxima with voltage intervals of 0.2 and 0.4 V were also observed. These CVCs correspond to the vibronic excitation of the adsorbed H_2O molecules [35]. Therefore, it can be concluded that during exposure to O_2, the HCO particles were oxidized to form H_2O molecules, which were then almost completely desorbed, and CO_2 molecules, some of which were adsorbed on the surface of nanoparticles. The exposure of the sample in oxygen also led to nickel oxidation, which manifested itself in an increase in the forbidden gap to ~2.6 eV on the CVCs of nanoparticles (curve *3*, Fig. 3b). On some Ni nanoparticles, the CVCs were recorded whose characteristics corresponded to the adsorbed particles of the formyl radical.

Thus, the effect of the interaction of nickel and gold nanoparticles shows itself in the fact that water is synthesized in a pronounced amount on the bimetallic coating and the oxidation of the formyl radical is partially prevented, which was not observed for the homogeneous coating based on gold nanoparticles.

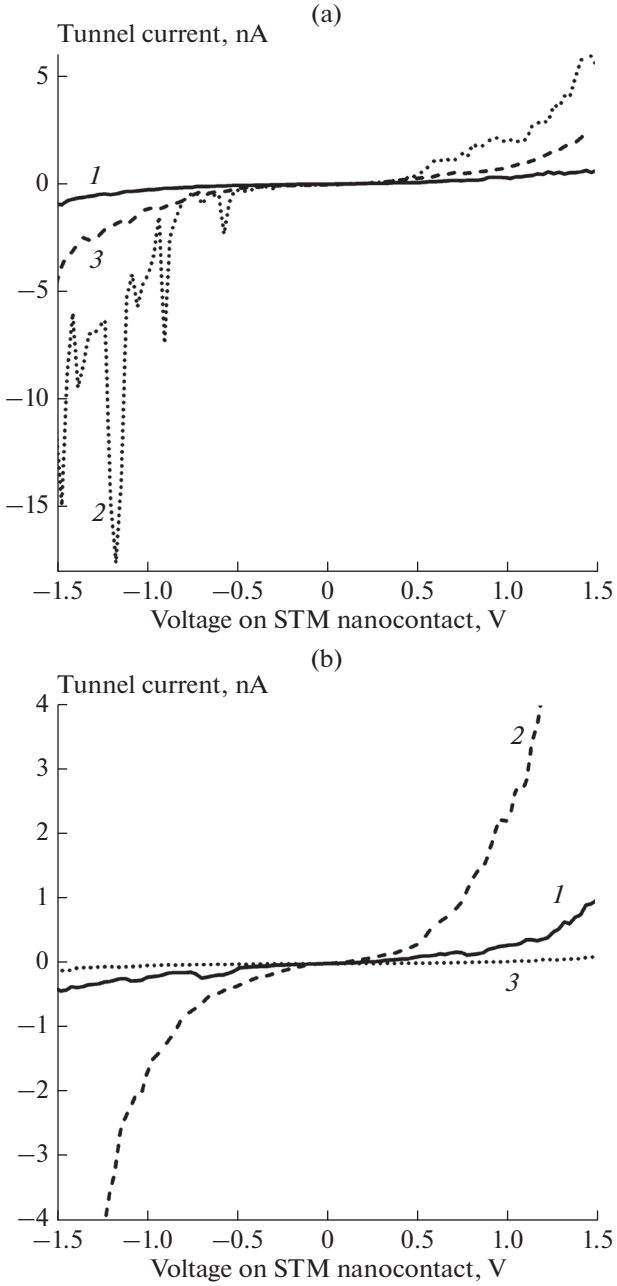

Fig. 3. Evolution of the electronic structure of (a) Au and (b) Ni nanoparticles as a result of interaction with gases. Both (a) and (b) show the curves measured after exposure in (*1*) H_2, (*2*) CO, and (*3*) O_2.

Nickel-Palladium Coating

An example of the image of the HOPG surface with a nanostructured coating formed by LED using a nickel-palladium $Ni_{0.65}Pd_{0.35}$ target is shown in Fig. 4. According to Fig. 4, the substrate contained a large number of almost spherical nanoparticles that were part of the clusters. The characteristic diameter of a cluster is ~60 nm; the coverage of the substrate is 12–15%, which is close to the calculated value. The average diameter of the clusters was determined to be 2–3 nm. The diameters of nanoparticles of the monometallic Ni and Pd coatings obtained by this method and studied earlier [16, 30] are exactly within this range. An analysis of the images of bimetallic NiPd nanoparticles deposited by laser electrodispersion from an alloy of a similar composition onto the TEM grids gave a slightly lower value, ~1 nm [24]. The discrepancy may be associated with the fact that the sizes of surface nanoobjects can increase by approximately the radius of the spherical STM tip during scanning. The surface of more than 90% of nanoparticles is covered with a semiconductor layer with a forbidden gap of ~1.5–2 eV. As the coating interacted with air, the semiconductor layer most likely includes nickel and palladium oxides. Examples of the CVCs of nanoparticles and HOPG are shown in Fig. 4b. Note that the E_g values of palladium oxide PdO strongly depend on the method of its preparation

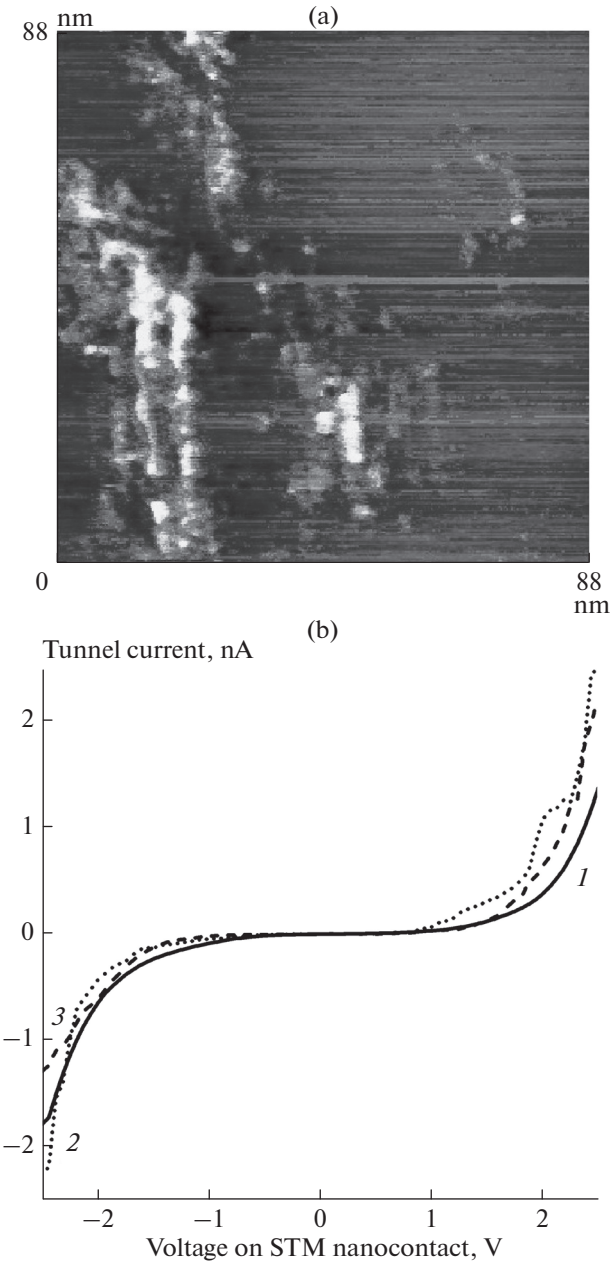

Fig. 4. Nickel–palladium coating on HOPG: (a) topographic image of a region of the surface; (b) CVCs of (*1*) HOPG and (*2*, *3*) examples of CVCs of nanoparticles.

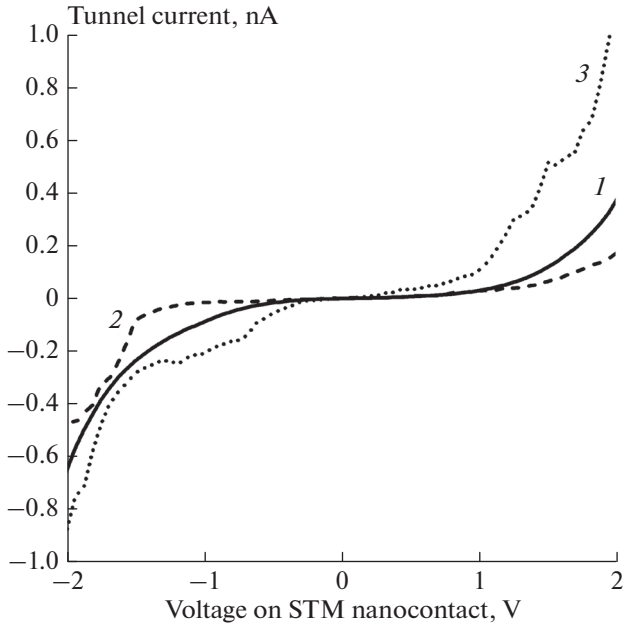

Fig. 5. Effect of adsorption on the electronic structure of nanoparticles of the nickel–palladium coating: CVCs of (*1*) HOPG and (*2, 3*) nanoparticles after exposure in (*2*) CO and (*3*) H_2.

and stoichiometry and vary from 2.13 eV [57] to 0.8 eV [58]; for coatings with a thickness increasing from 5 to 40 nm, E_g decreases from 2.3 to 2.15 eV [59].

The adsorption properties of the nickel–palladium nanostructured coating were determined with respect to CO and H_2. The exposure in CO led to a significant reduction in the forbidden gap to 0.6–0.8 on almost all nanoparticles (curve *2*, Fig. 5). Subsequent exposure to H_2 led to disappearance of the forbidden gap on the overwhelming majority of CVCs of nanoparticles (more than 85%) (curve *3*, Fig. 5). Thus, the exposure to CO and hydrogen led to a removal of oxides from the surface of nanoparticles. However, the forbidden band with a width of ~1 eV was preserved on ~15% of the curves even after prolonged heating of the sample in hydrogen at $T \approx 500$ K. Previous studies [30] of Ni nanoparticles deposited on HOPG by LED showed that nickel oxide is reduced under these conditions. These differences may be due to the interaction of the components of the bimetallic coating with each other and with the carbon support, which requires further research.

Our experiments did not allow us to separate the detected nanoparticles according to the elemental composition. It cannot be ruled out that the particles are formed by an alloy of nickel and palladium, as reported based on the energy dispersive analysis using TEM in [24]. This is also confirmed by the results of [60], which showed that a similar synthetic procedure forms exactly the nanoparticles of a nickel–palladium alloy.

CONCLUSIONS

The physicochemical properties of nanostructured coatings consisting of gold and copper, gold and nickel, and nickel and palladium were determined. The use of scanning tunnel microscopy combined with tunneling spectroscopy revealed that the AuCu and AuNi coatings consisted of gold, copper, and nickel nanoparticles, while mixed nanoparticles were

not detected. At the same time, the NiPd coating is possibly formed by nanoparticles consisting of these two elements. The adsorption properties of the above coatings with respect to hydrogen, carbon monoxide, and oxygen were determined. It was shown that the former two gases reduced the nanoparticle surface oxidized as a result of interaction with atmospheric oxygen. Hydrogen adsorption on pure gold and copper nanoparticles led to the transformation of their electronic structure from metal to semiconductor. The exposure of the gold and copper nanoparticles of the heterogeneous coatings in oxygen after hydrogen adsorption led to the partial removal of the latter in the water molecules.

ACKNOWLEDGMENTS

This study was performed under government contract no. 0082-2019-00 "Nanochemistry. Scientific principles of creation of new materials with given properties and functions including highly pure and nano materials" (AAAA-A20-120013190076-0) and partially supported by the Russian Foundation for Basic Research (grant nos. 18-53-00013 and 18-03-00060).

REFERENCES

1. O. G. Ellert, M. V. Tsodikov, S. A. Nikolaev, and V. M. Novotortsev, Russ. Chem. Rev. **83**, 718 (2014).
2. D. Kim, J. Resasco, Y. Yu, et al., Nat. Commun. **5**, 4948 (2014).
3. S. Neatu, J. A. Macia-Agullo, P. Concepcion, et al., J. Am. Chem. Soc. **136**, 15969 (2014).
4. R. He, Y. C. Wang, X. Y. Wang, et al., Nat. Commun. **5**, 4327 (2014).
5. C. L. Bracey, P. R. Ellis, and G. J. Hutchings, Chem. Soc. Rev. **38**, 2231 (2009).
6. T. Pasini, M. Piccinini, M. Blosi, et al., Green Chem. **13**, 2091 (2011).
7. C. della Pina, E. Falletta, and M. Rossi, J. Catal. **260**, 384 (2008).
8. J. C. Bauer, G. M. Veith, L. F. Allard, et al., ACS Catal. **2**, 2537 (2012).
9. J. Llorca, M. Dominguez, C. Ledesma, et al., J. Catal. **258**, 187 (2008).
10. L. Wang, Y. Zhong, H. Jin, et al., Beilstein J. Nanotechnol. **4**, 128 (2013).
11. X. Liu, A. Wang, L. Li, et al., J. Catal. **278**, 288 (2011).
12. S. A. Nikolaev, E. V. Golubina, I. N. Krotova, et al., Appl. Catal. B **168**, 303 (2015).
13. S. A. Nikolaev, E. V. Golubina, L. M. Kustov, A. L. Tarasov, and O. P. Tkachenko, Kinet. Catal. **55**, 311 (2014).
14. A. V. Chistyakov, P. A. Zharova, S. A. Nikolaev, et al., Catal. Today **279**, 124 (2017).
15. V. V. Smirnov, S. N. Lanin, A. Yu. Vasil'kov, S. A. Nikolaev, G. P. Murav'eva, L. A. Tyurina, and E. V. Vlasenko, Russ. Chem. Bull. **54**, 2286 (2005).
16. E. S. Lokteva, A. A. Peristyy, N. E. Kavalerskaya, et al., Pure Appl. Chem. **84**, 495 (2012).
17. R. Hou, W. Yu, M. D. Porosoff, et al., Catalysis **316**, 1 (2014).
18. M. S. Ahmed and S. Jeon, ACS Catal. **4**, 1830 (2014).
19. S. Maity and M. Eswaramoorthy, Mater. Chem. A **4**, 3233 (2016).
20. W. Ben Aziza, J. F. Petit, U. B. Demirci, et al., Int. J. Hydrogen Energy **39**, 16919 (2014).
21. S. U. Son, Y. Jang, J. Park, et al., J. Am. Chem. Soc. **126**, 5026 (2004).
22. R. Raja, V. B. Golovko, J. M. Thomas, et al., Chem. Commun., 2026 (2005).
23. N. Shang, X. Zhou, C. Feng, et al., Int. J. Hydrogen Energy **42**, 5733 (2017).
24. E. V. Golubina, T. N. Rostovshchikova, E. S. Lokteva, et al., Pure Appl. Chem. **90**, 1685 (2018). https://doi.org/10.1515/pac-2018-0207
25. G. N. Gerasimov, V. F. Gromov, M. I. Ikim, et al., Sens. Actuators, B **279**, 22 (2019).
26. V. I. Bukhtiyarov and M. G. Slin'ko, Russ. Chem. Rev. **70**, 147 (2001).
27. T. N. Rostovshchikova, M. I. Shilina, E. V. Golubina, E. S. Lokteva, I. N. Krotova, S. A. Nikolaev, K. I. Maslakov, and D. A. Yavsin, Russ. Chem. Bull. **64**, 812 (2015).
28. A. V. Chistyakov, P. A. Zharova, S. A. Nikolaev, et al., Catal. Today **279**, 124 (2017).
29. T. V. Belysheva, A. K. Gatin, M. V. Grishin, M. I. Ikim, V. M. Matyuk, S. Y. Sarvadii, L. I. Trakhtenberg, and B. R. Shub, Russ. J. Phys. Chem. B **9**, 733 (2015).
30. A. K. Gatin, M. V. Grishin, S. A. Gurevich, N. V. Dokhlikova, A. A. Kirsankin, V. M. Kozhevin, E. S. Lokteva, T. N. Rostovshchikova, S. Yu. Sarvadii, B. R. Shub, and D. A. Yavsin, Nanotechnol. Russ. **10**, 850 (2015).
31. A. K. Gatin, M. V. Grishin, S. A. Gurevich, N. V. Dokhlikova, A. A. Kirsankin, V. M. Kozhevin, N. N. Kolchenko, T. N. Rostovshchikova, V. A. Kharitonov, B. R. Shub, and D. A. Yavsin, Russ. Chem. Bull. **63**, 1696 (2014).
32. M. V. Grishin, A. K. Gatin, V. G. Slutskii, V. A. Kharitonov, and B. R. Shub, Russ. J. Phys. Chem. B **9**, 596 (2015).
33. N. V. Dokhlikova, M. V. Grishin, S. Yu. Sarvadii, and B. R. Shub, Russ. J. Phys. Chem. B **13**, 525 (2019).
34. T. N. Rostovshchikova, V. V. Smirnov, V. M. Kozhevin, et al., Ross. Nanotekhnol. **2** (1–2), 47 (2007).
35. M. V. Grishin, A. K. Gatin, N. V. Dokhlikova, A. A. Kirsankin, A. I. Kulak, S. A. Nikolaev, and B. R. Shub, Kinet. Catal. **56**, 532 (2015).
36. A. A. Gatin, M. V. Grishin, N. V. Dokhlikova, S. A. Ozerin, S. Yu. Sarvadii and B. R. Shub, Nanotechnol. Russ. **13**, 453 (2018).
37. L. Wang, Y. Zhong, H. Jin, et al., Beilstein J. Nanotechnol. **4**, 111 (2013).
38. D. Tahir and S. Tougaard, J. Phys.: Condens. Mater. **24**, 175002 (2012).
39. F. P. Koffyberg and F. A. Benko, J. Appl. Phys. **53**, 1173 (1982).
40. I. V. Morozov, K. O. Znamenkov, Y. M. Korenev, et al., Thermochim. Acta **403**, 173 (2003).

41. J. Han, Y. Zahou, Y.-Q. Chai, et al., Talanta **85**, 130 (2011).
42. J. Wang, J. Li, A. J. Baca, et al., Anal. Chem. **75**, 3941 (2003).
43. L. Rout, A. Kumar, R. S. Dhaka, et al., Appl. Catal., A **538**, 107 (2017).
44. W. Zhan, J. Wang, H. Wang, et al., J. Am. Chem. Soc. **139**, 8846 (2017).
45. Y. Li and P. A. Korzhavyi, Dalton Trans. **46**, 529 (2017).
46. V. Maurya, G. Sharma, U. Paliwal, et al., Comput. Mater. Sci. **150**, 329 (2018).
47. E. Bennett, T. Wilson, P. J. Murphy, et al., Inorg. Chem. **54**, 2213 (2015).
48. A. K. Gatin, M. V. Grishin, S. Yu. Sarvadii, and B. R. Shub, Russ. J. Phys. Chem. B **12**, 317 (2018).
49. M. V. Grishin, A. K. Gatin, S. Yu. Sarvadii, and B. R. Shub, Nanotechnol. Russ. **12**, 589 (2017).
50. P. S. Patil and L. D. Kadam, Appl. Surf. Sci. **199**, 211 (2002).
51. G. Boschloo and A. Hagfeldt, J. Phys. Chem. B **105**, 3039 (2001).
52. W. Brockner, C. Ehrhardt, and M. Gjikaj, Thermochim. Acta **456**, 64 (2007).
53. K. M. Ostyn and C. B. Carter, Surf. Sci. **121**, 360 (1982).
54. M. M. Wohar and P. W. Jagodzinski, J. Mol. Spectrosc. **148**, 13 (1991).
55. M. Rothaemel, H. W. Zanthoff, and M. Baerns, Catal. Lett. **28**, 321 (1994).
56. M. Fastow, Y. Kosirovski, and M. Folman, J. Electron. Spectrosc. Relat. Phenom. **64–65,** 643 (1993).
57. E. Rey, M. R. Kamal, R. B. Miles, et al., J. Mater. Sci. **13**, 812 (1978).
58. P. O. Nilsson and M. S. Shivaraman, J. Phys. C **12**, 1423 (1979).
59. S. V. Ryabtsev, V. M. Ievlev, A. M. Samoylov, et al., Thin Solid Films **636**, 751 (2017).
60. R. Mahfouz, F. Cadete Santos Aires, A. Brenier, et al., J. Nanopart. Res. **12**, 3123 (2010).

Translated by L. Smolina

SPELL: 1. OK